Numerical simulation of central shrinkage crack formation in a 234-t steel ingot

Jing-an Yang[1], Yue-qiao Wang[2], *Hou-fa Shen[1], and Bai-cheng Liu[1]

1. School of Materials Science and Engineering, Tsinghua University, Beijing 100084, China

2. Casting and Forging Workshop, China National Erzhong Group Co. Ltd., Deyang 618000, China

Abstract: Central shrinkage crack is a common defect encountered in steel ingot casting. It is necessary to limit the degree of crack in case of further propagation in forging. A 234-t steel ingot was dissected to check the internal quality, and a central shrinkage crack band of 1,400 mm in height and 120 mm in width, was found at a distance of 450 mm under the riser bottom line. Then, thermo-mechanical simulation using an elasto-viscoplastic finite-element model was conducted to analyze the stress-strain evolution during ingot solidification. A new criterion considering mush mechanical property in the brittle temperature range as well as shrinkage porosity was used to identify the shrinkage crack potential, where the degree of shrinkage porosity is regarded as a probability factor using a modified sigmoid function. Different casting processes, such as pouring speed, mould preheating and riser insulation, were optimized with the simulation model. The results show that fast pouring, proper mould preheating and good riser insulation can alleviate shrinkage crack potential in the ingot center.

Key words: shrinkage crack; finite-element; crack potential; thermo-mechanical simulation; steel ingot

CLC numbers: TP391.99 **Document code:** A **Article ID:** 1672-6421(2017)05-365-08

Central shrinkage crack in steel ingot is a hot tear caused by the shrinkage during solidification, and it differs from the porosity as for its shape. Controlling its magnitude and degree by optimizing the casting process is a precaution for subsequent processing. As explained by Stangeland et al [1], this defect is a result of inadequate melt feeding initiating cracks and severe deformation leading to the opening and propagation of the cracks. Won et al. [2] also pointed out that in the brittle temperature range (BTR), the solidifying steel begins behaving like a solid, but the steel is very susceptible to hot crack due to the presence of the interdendritic liquid films caused by the microsegregation of solute elements.

Monroe et al. [3] studied various "T" shaped steel castings and suggested that reducing the strain in the casting and increasing the feeding of the section would decrease the hot tear tendency. Olivier et al. [4] analyzed two kinds of tests, such as constrained solidification test and ingot bending test, to study how cracks occur and propagate during the solidification of steel and found that the tears initiate in subsurface zones of the hot spot and propagate or not as solidification proceeds. Koshikawa et al. [5] applied a deformation at the surface of a solidifying 450-kg steel ingot and integrated a hot tearing criterion that compares the local accumulation of strain with the expression of a critical value. Wei et al. [6] developed an apparatus for real-time measuring the contraction stress and temperature during solidification, which can achieve the in-situ observation of melting and solidification and find the largest hot tearing susceptibility temperature range. Yang et al. [7] inspected internal crack in a 6-ton steel ingot by X-ray high energy industrial CT and found that the interconnected defects derived from continuous liquid films, and then were torn apart by the excessive tensile stress in the BTR.

Various criteria have been proposed aiming at the prediction of crack initiation since the early 1960s [8]. These criteria mainly focus on the shrinkage crack susceptibility, i.e., the potential of shrinkage crack formation, which can be classified into three main categories. First, it is non-mechanical criteria, such as Clyne and Davies' and Katgerman's criteria [9], which are defined by the ratio of vulnerable period where shrinkage crack may develop and time available for the stress relief process where mass feeding and liquid feeding occur. Second, it is mechanical criteria, such as Prokhorov, Novikov, Sczygiol, WYSO (Won-Yeo-

***Hou-fa Shen**

Male, born in 1964, Ph.D., Professor. Research interests: modeling and simulation of solidification process related to casting.

E-mail: shen@tsinghua.edu.cn

Received: 2017-08-15; Accepted: 2017-09-20

Seol-Oh) and CBC (Cerri-Bellet-Chastel) criteria [2, 9-12], which stress on critical strain or strain rate in relation to the fracture strain or strain rate of the mush zone in the BTR. Finally, it is a combination of both non-mechanical and mechanical criteria, such as RDG (Rappaz-Drezet-Gremaud) and Suyitno criteria [13, 14], which investigate the pressure drop over the mush zone reaching a critical value for cavity nucleation or the microporosity exceeding a critical size.

In this work, an experiment was carried on a 234-t heavy steel ingot where a shrinkage crack band was found in the ingot upper centerline. Thermo-mechanical simulation based on ProCAST software considering gap formation was carried out to study the temperature field evolution, shrinkage porosity and principal stress-strain evolution. Through C++ programming with the extracted results from ProCAST, a shrinkage crack potential (SCP) criterion is proposed. Then, various casting processes are quantitatively evaluated by the new criterion and optimizing casting technologies are suggested.

1 Experiment

A 234-t heavy steel ingot cast by China National Erzhong Group was dissected to check the internal quality. The ingot was top vacuum poured in a mould with twenty-four edges, 5,780 mm in height, and 2,910 mm in mean diameter. Grade of the ingot was a low alloy steel 12Cr-2Mo-1V with the composition listed in Table 1.

Schematic of the ingot and mould system is depicted in Fig. 1(a) with four parts, i.e., mould, insulation tiles, anti-piping compounds and ingot. The ingot body on the half was sliced into three plates on the center longitudinal plane. A central shrinkage crack band, 1,400 mm in height and 120 mm in width, was found at a distance of 450 mm under the riser bottom line as shown in Fig. 1(b). From the enlarged view, the shrinkage crack band consists of many small cracks, which were seemingly intermittent, but more continuous in the whole crack zone. As the solidification processes, the ingot core shows inadequate feeding as well as tensile deformation. Liquid films form between the dendrites network and develop into shrinkage pores and shrinkage cracks. The greater the tensile deformation, the more the shrinkage cracks will form.

Table 1: Composition of steel 12Cr-2Mo-1V (wt.%)

C	Mn	Si	P	S	Cr	Mo	Ni	V	Fe
0.146	0.56	0.05	0.006	0.003	2.425	1.05	0.205	0.32	Bal.

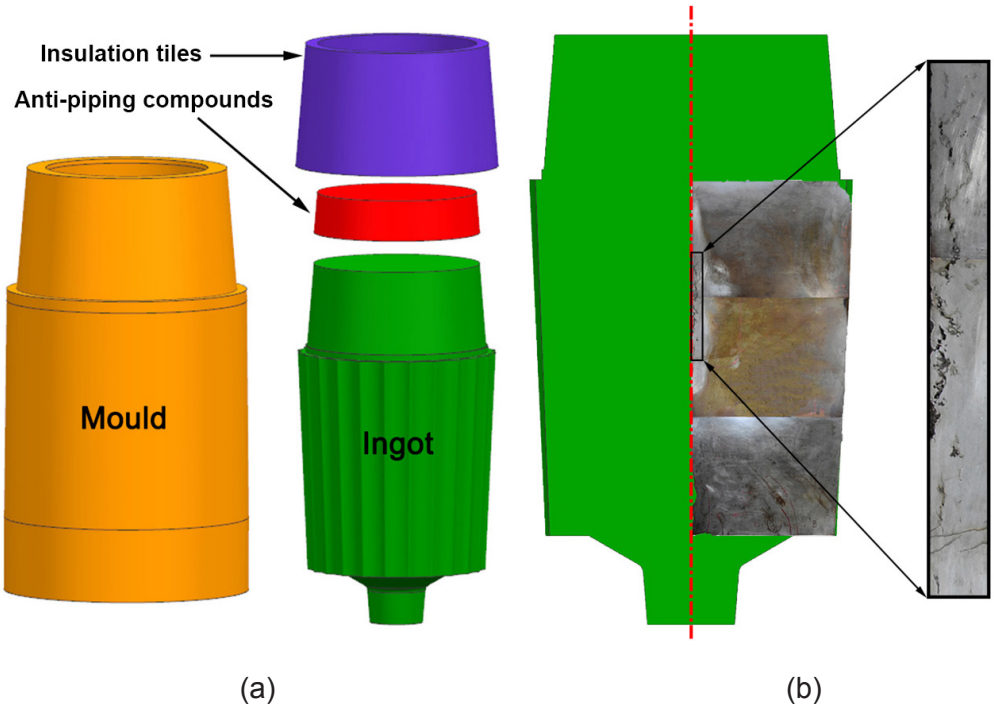

Fig. 1: (a) Schematic of ingot and mould system, (b) part of sliced ingot including a central shrinkage crack band with a close-up

2 Numerical simulation

2.1 3D FEM thermo-mechanical simulation

A 3D FEM mesh with 239,469 nodes and 1,385,595 elements was generated for the thermo-mechanical simulation of the 234-t ingot based on ProCAST software, as shown in Fig. 2. An elasto-viscoplastic model based on the Perzyna model was used for the stress type of 12Cr-2Mo-1V steel. In the Perzyna model, evolution of the viscoplastic strain rate is defined, as shown in Equation (1):

$$\dot{\varepsilon}^{vp} = \frac{1}{\eta}\left(\frac{\sigma-\sigma_s}{\sigma^*}\right)^p \qquad \begin{cases}\sigma > \sigma_s & \dot{\varepsilon}^{vp} \neq 0\\ \sigma \le \sigma_s & \dot{\varepsilon}^{vp} = 0\end{cases} \qquad (1)$$

where η is the viscous parameter, p is the viscous power, σ-σ_s is the stress level of the plateau minus the flow stress σ_s, and σ^* equals 1 MPa [15]. The flow stress analysis under different temperatures and strain rates was performed on general database of JmatPro. Then, the viscous parameter, η, and the viscous power, p, in the elasto-viscoplastic model were calculated.

Thermo-physical properties of the 12Cr-2Mo-1V steel, such as heat conductivity, density, enthalpy and the solid fraction were calculated using CompuTherm thermodynamic database of ProCAST for multi-component Fe-rich alloys. These thermo-physical parameters are temperature dependent, as shown in Fig. 3. Additional thermo-mechanical properties, such as Poisson's ratio and thermal expansion, are calculated by CompuTherm as well. Figure 4(a-e) shows the temperature dependent thermo-mechanical parameters. Additionally, Fig. 4 (f) displays their values in the temperature range between 550 °C and 1,450 °C, where the left vertical axis is logarithmic axis and represents the viscous parameter η, and the right vertical axis is normal axis and represents the viscous power p.

In the calculation, the exothermic ratio of anti-piping compounds was set as 1, 897.3 kJ·kg^{-1}. The ingot mould was made of HT150 gray cast iron and its stress type was set as rigid. The insulation tiles' property was from the factory test and its stress type was set as rigid. Appropriate thermal boundary, mechanical boundary, and interface conditions were set for the simulation, where different pouring speeds, mould preheating and riser insulation were considered.

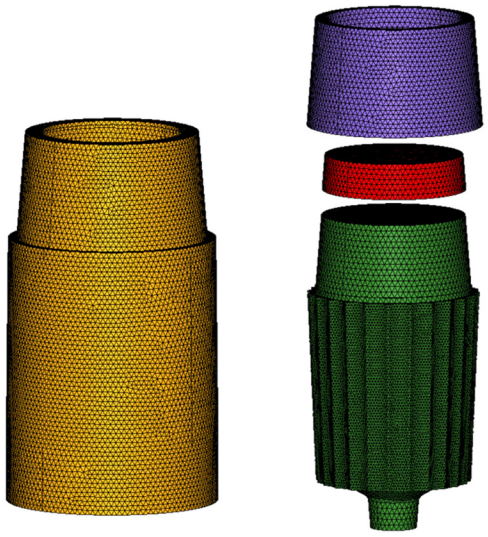

Fig. 2: 3D FEM mesh of 234 t ingot and mould system

During the thermo-mechanical calculation, the gap model assumes that heat conduction through the air gap is progressively replacing the heat transfer coefficient due to the contact. When there is a contact, the heat transfer coefficient is increased as a function of the pressure, as shown in Equation (2):

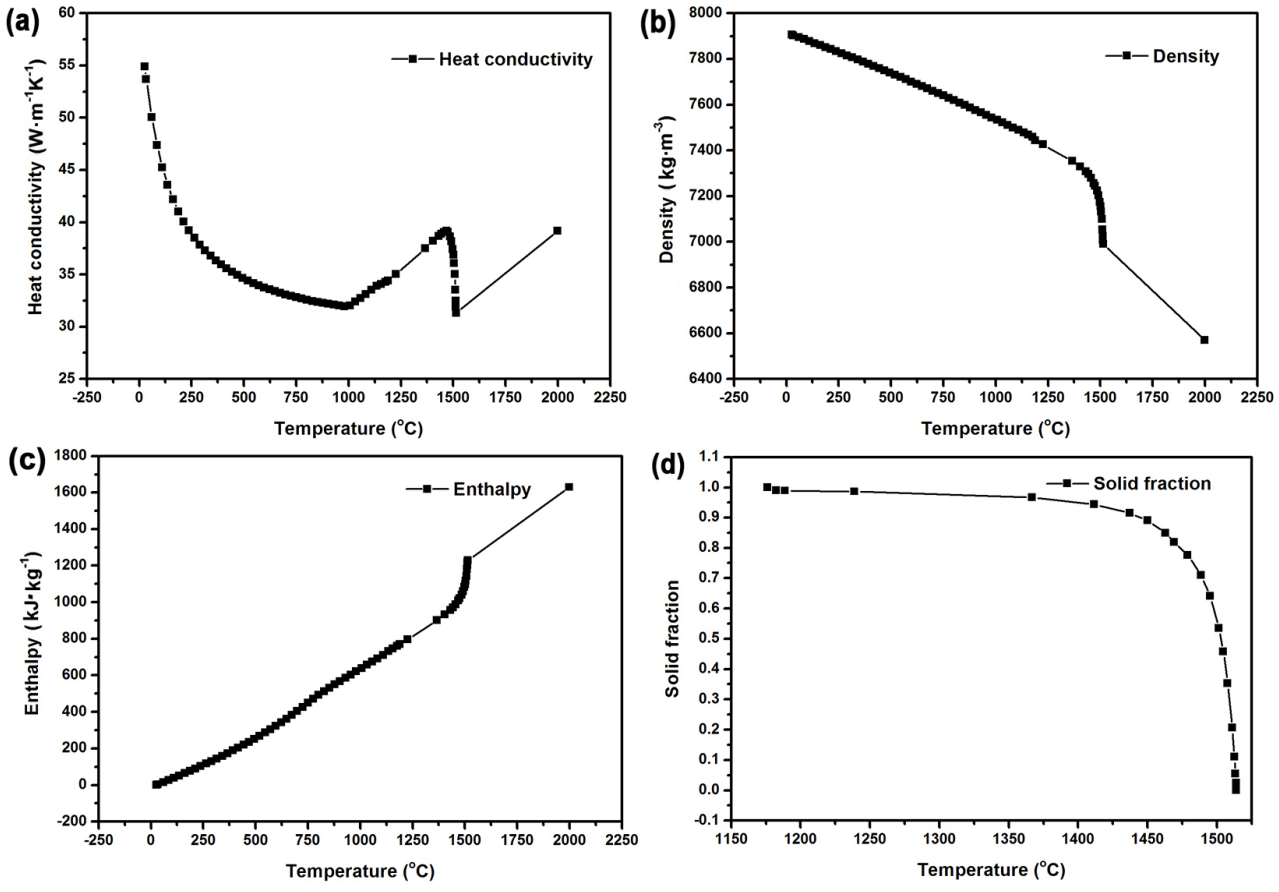

Fig. 3: Curves of thermo-physical parameters with temperature: (a) heat conductivity, (b) density, (c) enthalpy, (d) solid fraction

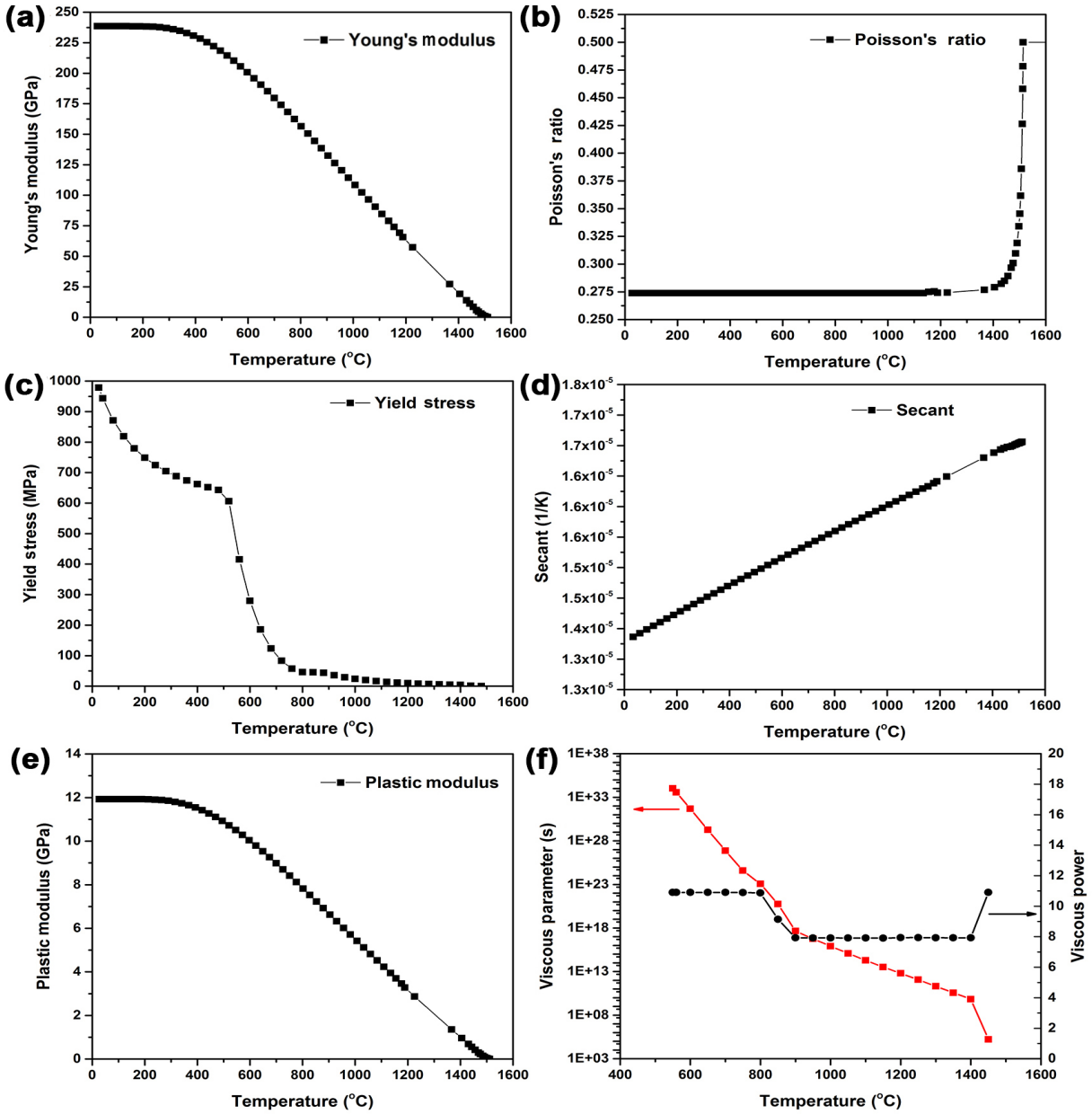

Fig. 4: Curves of thermo-mechanical parameters with temperature: (a) Young's modulus, (b) Poisson's ratio, (c) yield stress, (d) secant thermal expansion coefficient, (e) plastic modulus, (f) viscous parameter and viscous power

$$h = h_0 \cdot \left(1 + \frac{P}{A}\right) \tag{2}$$

where h is the adjusted heat transfer coefficient, h_0 is the initial value of the heat transfer coefficient, P is the contact pressure, and A is an empirical constant to account for the contact pressure. When the gap is formed, the heat transfer coefficient is defined as shown in Equation (3):

$$h = \frac{1}{1/h_0 + R_{gap}} \quad \text{with} \quad R_{gap} = \frac{1}{k/gap + h_{rad}} \tag{3}$$

where R_{gap} is the thermal resistance of air gap, k is the conductivity of air, gap is the air gap width, and h_{rad} is the radiative equivalent heat transfer coefficient.

2.2 Shrinkage crack potential

After completing solidification computation of the ingot, data of the FEM mesh, temperature field evolution, the cooling rate, shrinkage porosity and principal stress-strain evolution in three directions were extracted from the simulation results. Subsequently, the extracted data was further processed by C++ programming to evaluate shrinkage crack potential (SCP) throughout the ingot.

Since the mushy state mechanical behavior plays an important role in the formation of shrinkage crack, a viscoplastic constitutive model relating the dynamic yield stress to the viscoplastic strain and strain rate was used to contrast with the simulated results by the Perzyna model, as shown in Equation (4):

$$\sigma_{dy} = \sigma_0 \left(1 + \frac{\varepsilon_{eq}}{\varepsilon_0}\right)^n \left(1 + \frac{\dot{\varepsilon}_{eq}}{\dot{\varepsilon}_0}\right)^m \tag{4}$$

where σ_0 is the initial yield stress, n is the strain hardening exponent, m is the strain rate sensitivity exponent, ε_{eq} is the

equivalent plastic strain, and $\dot{\varepsilon}_{eq}$ is the equivalent strain rate [16]. The reference shear strain, ε_0, the reference shear strain rate, $\dot{\varepsilon}_0$, and the equivalent strain rate, $\dot{\varepsilon}_{eq}$, are given in Equations (5)–(7):

$$\varepsilon_0 = \frac{\sigma_0 n}{E} \tag{5}$$

$$\dot{\varepsilon}_0 = Ae^{-Q/RT} \tag{6}$$

$$\dot{\varepsilon}_{eq} = \frac{\varepsilon_{eq}}{BTR}\dot{T} \tag{7}$$

where E is the Young's modulus, A is a prefactor, Q is the activation energy, R is the universal gas constant, $\dot{T}$ is the cooling rate, and BTR is the brittle temperature range.

Inadequate feeding and tensile deformation are two essential factors for the formation of shrinkage crack. Thus, the degree of shrinkage porosity was regarded as a probability factor of the crack formation using a modified sigmoid function. The sigmoid function is a threshold function having a characteristic "s" shaped curve. The value ranges from zero to one. Equation (8) presents the modified sigmoid function:

$$P = \frac{1}{1+e^{-\mathrm{A}(sp-\mathrm{B})}} \tag{8}$$

where P is the probability factor of shrinkage crack formation, sp is the shrinkage porosity, and A and B are constants that need to be calibrated. The probability factor monotonically increases from zero to one. Assuming that when shrinkage porosity is less than 2.4%, the probability factor of shrinkage crack tends toward zero, i.e. when sp=2.4%, $P<10^{-3}$. This means there is adequate melt feeding for the healing of possible shrinkage pores or cracks even if it is under a great amount of tensile deformation. In addition, assuming that when shrinkage porosity is more than 4.2%, the probability factor of shrinkage crack tends toward one, i.e. when sp=4.2%, $1-P<10^{-3}$. That means the porous mushy zone is very inclined to propagate shrinkage pore chains or cracks under enough tensile deformation. From Equation (9), it can be deducted that A>7.67 and B>3.26. Therefore, A was set as 8 and B was set as 3.3.

$$\begin{cases} \dfrac{1}{1+e^{-\mathrm{A}(2.4-\mathrm{B})}} < 10^{-3} \\ 1-\dfrac{1}{1+e^{-\mathrm{A}(4.2-\mathrm{B})}} < 10^{-3} \end{cases} \tag{9}$$

The function curve is plotted in Fig. 5, where point (3.3, 0.5) is the symmetry center of the "s" shaped curve.

Taking account of the shrinkage porosity, mush state mechanical behavior and stress-strain evolution in the BTR, a criterion was proposed to evaluate the shrinkage crack potential, as shown in Equation (10):

$$SCP = \underset{BTR}{Max}\left(\frac{\sigma_1}{\sigma_{dy}}\right)\cdot\frac{1}{1+e^{-8(sp-3.3)}} \tag{10}$$

where SCP is the shrinkage porosity potential, BTR is the brittle temperature range, σ_1 is the first principal stress, σ_{dy} is the dynamic yield stress, and sp is the shrinkage porosity.

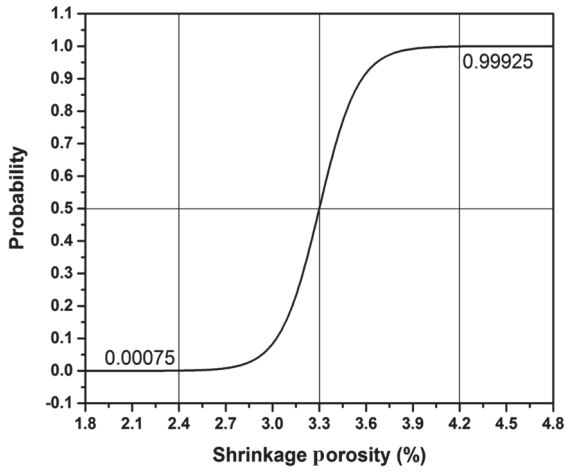

Fig. 5: Relationship between the probability factor of shrinkage crack formation and the shrinkage porosity

3 Results and discussion

3.1 Model validation

According to the practice, a 3D FEM model was built for the thermo-mechanical analysis of the 234t ingot based on ProCAST. Then data of the FEM mesh, the temperature field evolution, the cooling rate, the shrinkage porosity and principal stress-strain evolution in three directions were extracted and processed by C++ programming to evaluate shrinkage crack potential by the SCP criterion throughout the ingot.

Figure 6 shows the simulated results, such as shrinkage porosity and SCP, compared with the experiment results on the longitudinal ingot plane. It can be seen from Fig. 6(b) that the shrinkage pipe bottom and the ingot upper centerline bear the most serious shrinkage porosity. In addition, the simulated central shrinkage porosity band was longer than the experimental central shrinkage crack band. They were aligned at the bottom, but the former was more close to the riser. Figure 6(c) shows the contour map of maximum σ_1/σ_{dy} in the BTR. It can be seen that the tensile stress developed a lot along the ingot centerline in the BTR, especially in the lower centerline and riser center. The lower part of the ingot has enough melt feeding and the cracks developed in this area could be healed to some extent. The SCP criterion considers shrinkage porosity as a probability factor, and additionally it takes mush state mechanical behavior and stress-strain evolution in the BTR into account. As seen from Fig. 6(d), the shrinkage pipe bottom and the ingot upper centerline bear the greatest shrinkage crack potential. Therefore, the thermo-mechanical model with SCP criterion is able to make a valid prediction of the shrinkage crack formation.

3.2 Process optimization

3.2.1 Pouring speed

In order to quantitatively describe the shrinkage crack potential in the ingot center zone and compare different simulation results with different pouring parameters, a statistical model was used to assess the steel ingot quality. Since the ingot body quality is of most concern, it counts the SCP values in the ingot body identified by a black box, as shown in Fig. 6(d). Two statistical indexes, i.e., average of SCP (E) and standard deviation of SCP (D), are calculated. E indicates the magnitude of shrinkage crack potential, while D indicates the discretization degree of shrinkage crack potential. The greater the value of E, the worse the ingot body quality. When the E values are close to each other, the greater the D value, the more the shrinkage crack potential is discrete. This means there are more and greater SCP values above the average level, which is detrimental to the ingot body quality.

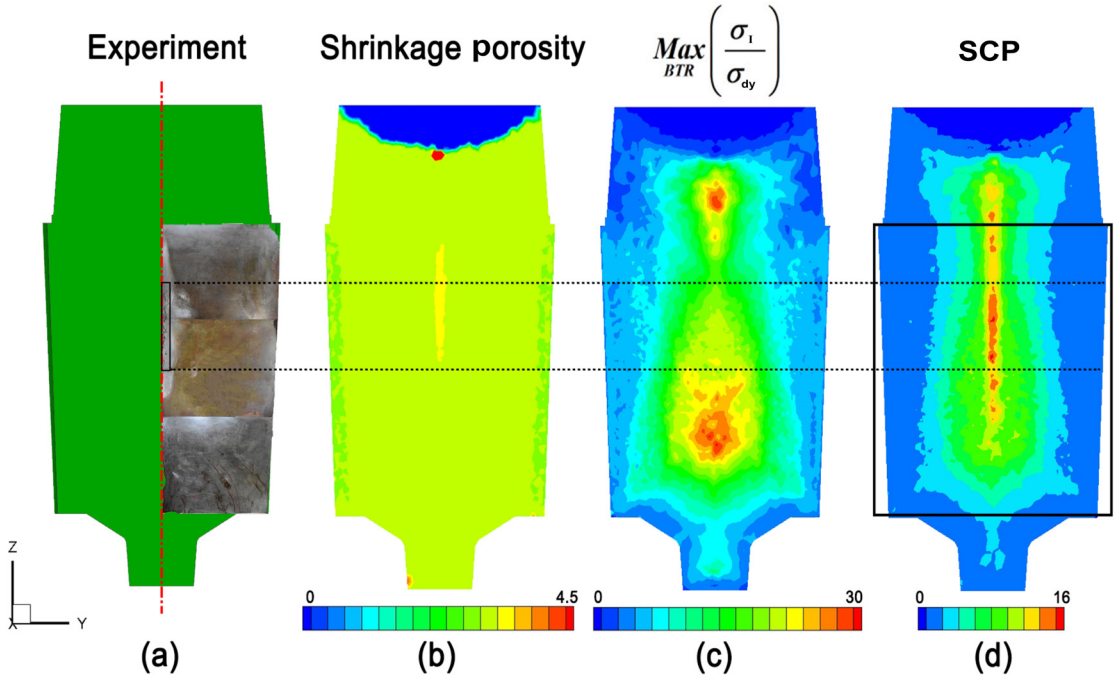

Fig. 6: (a) Experiment results showing part of sliced ingot, (b) simulated shrinkage porosity, (c) maximum σ_I/σ_{dy} in *BTR*, (d) shrinkage crack potential (SCP) on longitudinal ingot plane

To investigate pouring speed separately, the melt with superheat of 50°C was poured at speeds of 300, 500, and 700 kg·s^{-1}, respectively. The statistical SCP indexes with different pouring speeds are summarized in Fig. 7(a), and relevant simulated SCP results with different pouring speeds are shown in Fig. 7(b). It can be seen from Fig. 7(a) that the average of SCP decreases with the increase of pouring speed, and standard deviation of SCP fluctuates in a small range. The average of SCP with pouring speed of 700 kg·s^{-1} is slightly lower than that of 500 kg·s^{-1}. Therefore, pouring at a sufficiently high speed can alleviate shrinkage crack potential in the ingot center.

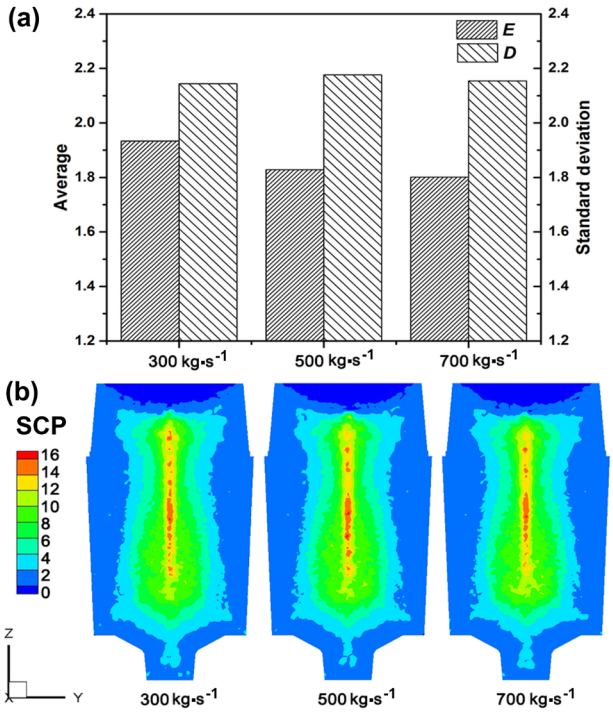

Fig. 7: (a) Statistical SCP indexes with different pouring speeds, (b) Simulated SCP results with different pouring speeds

3.2.2 Mould preheating

To investigate the effect of mould preheating on the shrinkage crack potential, the ingot mould initial temperature is set at 20 °C, 200 °C, and 300 °C, respectively. The statistical SCP indexes with different mould preheating temperatures are summarized in Fig. 8(a) and relevant simulated SCP results with different pouring temperatures are shown in Fig. 8(b). It can be seen from Fig. 8(a) that the SCP average decreases with the increase of mould preheating temperature. Meanwhile, standard deviation of SCP decreases as well. The average of SCP and

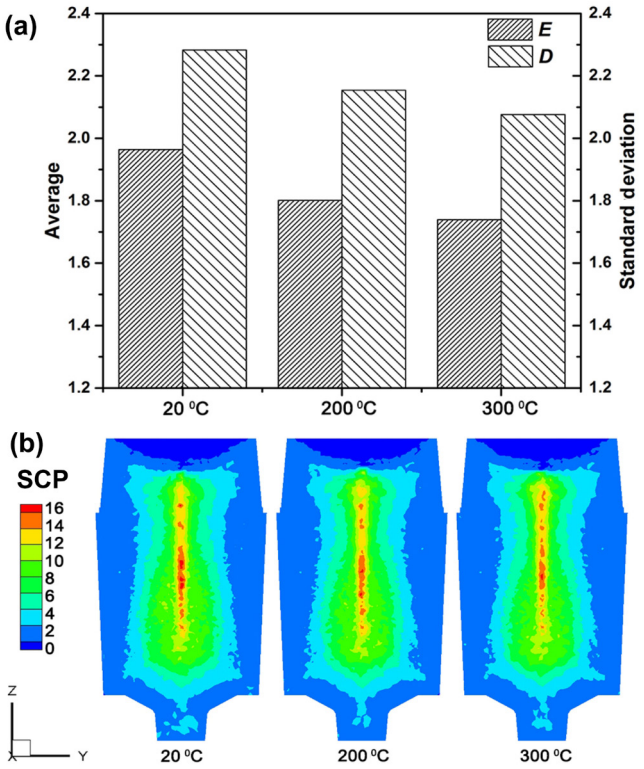

Fig. 8: (a) Statistical SCP indexes with different mould preheating temperatures, (b) Simulated SCP results with different mould preheating temperatures

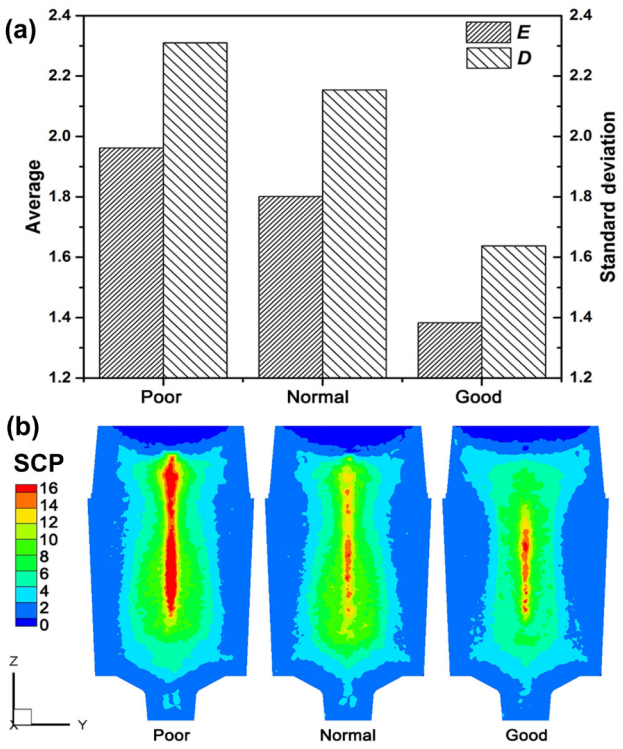

Fig. 9: (a) Statistical SCP indexes with different riser insulation conditions, (b) Simulated SCP results with different riser insulation conditions

standard deviation of SCP when mould preheating is 300 °C are slightly lower than that at 200 °C. Considering the high cost of heating ingot mould, proper mould preheating (e.g. 200 °C) is sufficiently beneficial to the ingot body quality.

3.2.3 Riser insulation

To investigate the riser insulation effect on the shrinkage crack potential, the insulation condition for the ingot riser is set as poor, normal, and good, respectively. The statistical SCP indexes with different riser insulation conditions are summarized in Fig. 9(a) and relevant simulated SCP results with different riser insulation conditions are shown in Fig. 9(b). As shown in Fig. 9(a), both average of SCP and standard deviation of SCP decrease sharply with the enhancement of riser insulation. Therefore, in the permitted conditions, riser insulation should be improved as much as possible.

4 Conclusions

(1) A 234-t 12Cr-2Mo-1V steel ingot was cast and dissected to check the internal quality. It was found that a central shrinkage crack band, 1,400 mm in height and 120 mm in width, locates at a distance of 450 mm under the riser bottom line.

(2) An elasto-viscoplastic model was used for the stress type of 12Cr-2Mo-1V. Database of JmatPro and CompuTherm thermodynamic database of ProCAST were used to calculate the materials' thermo-physical and thermo-mechanical properties. Additionally, 3D FEM thermo-mechanical simulation, based on ProCAST software considering gap formation, was carried out to study the temperature field evolution, the shrinkage porosity, and principal stress-strain evolution.

(3) Taking account of the shrinkage porosity, mush state mechanical behavior, and stress-strain evolution in the BTR, a criterion named shrinkage crack potential (SCP) was proposed to evaluate the shrinkage crack potential, in which the degree of the shrinkage porosity was regarded as a probability factor using a modified sigmoid function. It was realized by C++ programming with the extracted results from ProCAST. Two statistical indexes, i.e., average of SCP, E, and standard deviation of SCP, D, were used to quantitatively describe the shrinkage crack potential in the ingot center zone, under different casting processes.

(4) The simulation results show that pouring at a sufficient high speed, proper mould preheating, and improving riser insulation as much as possible can alleviate the shrinkage crack potential in the ingot center, improving the ingot inner quality. Further efforts should be carried on finer thermo-mechanical model, considering composition segregation and grain structures, to make more sound prediction of the shrinkage crack formation.

References

[1] Stangeland A, Mo A, M'Hamdi M, et al. Thermal strain in the mushy zone related to hot tearing. Metallurgical and Materials Transactions A, 2006, 37A(3): 705.

[2] Won Y M, Yeo T, Seol D J, et al. A new criterion for internal crack formation in continuously cast steels. Metallurgical and Materials Transactions B, 2000, 31(4): 779–794.

[3] Monroe C, Beckermann C. Development of a hot tear indicator for steel castings. Materials Science and Engineering: A, 2005, 413–414: 30–36.

[4] Olivier C, Yvan C, Michel B. Hot tearing in steels during solidification: experimental characterization and thermomechanical modeling. Journal of Engineering Materials and Technology, 2008, 130(2): 21018.

[5] Koshikawa T, Bellet M, Gandin C, et al. Study of hot tearing during steel solidification through ingot punching test and its numerical simulation. Metallurgical and Materials Transactions A, 2016, 47(8): 4053–4067.

[6] Wei Zhiqiang, Chen Xiangru, Zhong Honggang, et al. Hot tearing susceptibility of Fe-20.96Cr-2.13Ni-0.15N-4.76Mn-0.01Mo duplex stainless steel. Journal of Iron and Steel Research International, 2017, 24(4): 421–425.

[7] Yang Jingan, Shen Houfa, Liu Baicheng, et al. Analysis of internal crack in a six-ton P91 ingot. China Foundry, 2016, 13(3): 191–198.

[8] Eskin D G, Katgerman L. A quest for a new hot tearing criterion. Metallurgical and Materials Transactions A, 2007, 38(7): 1511–1519.

[9] Suyitno, Kool W H, Katgerman L. Hot tearing criteria evaluation for direct-chill casting of an Al-4.5 pct Cu alloy. Metallurgical and Materials Transactions A, 2005, 36(6): 1537–1546.

[10] Bellet M, Cerri O, Bobadilla M, et al. Modeling hot tearing during solidification of steels: assessment and improvement of macroscopic criteria through the analysis of two experimental tests. Metallurgical and Materials Transactions A, 2009, 40(11): 2705–2717.

[11] Sczygiol N. A new stress criterion for hot-tearing evaluation in solidifying casting. Acta Mechanica et Automatica, 2012, 4(6): 56–62.

[12] Poltarak G, Ferro S, Cicutti C. Estimation of internal cracking risk in the continuous casting of round bars. Steel Research International, 2017, 88(4): 1600223.

[13] Rappaz M, Drezet J M, Gremaud M. A new hot-tearing criterion. Metallurgical and Materials Transactions A, 1999, 30(2): 449–455.

[14] Suyitno, Kool W H, Katgerman L. Integrated approach for prediction of hot tearing. Metallurgical and Materials Transactions A, 2009, 40(10): 2388–2400.

[15] ProCAST [computer program] Version 2014.0, ESI Group, France.

[16] Galles D, Monroe C A, Beckermann C. Measurement and simulation of deformation and stresses in steel casting. MCWASP, Schladming, Austria, 2012, 33, 012049.

This work was financially supported by the NSFC-Liaoning Joint Fund (U1508215) and the project to strengthen industrial development at the grass-roots level of MIIT China (TC160A310/21).